Chemical Science

ROYAL SOCIETY OF CHEMISTRY

EDGE ARTICLE

View Article Online
View Journal

Cite this: DOI: 10.1039/d5sc08656f

All publication charges for this article have been paid for by the Royal Society of Chemistry

Acidic *in vitro* selection of metal-specific deoxyribozymes

Pan Jia,[a] Yangyang Chang,*[ab] Shen Li,[b] Wei Xue,[a] Shusen Xiao,[a] Qiang Zhang,[c] Jiuxing Li,[ab] Ying Wang,[d] Zijie Zhang*[ab] and Meng Liu*[ab]

Deoxyribozymes (DNAzymes) are *in vitro* selected catalytic DNA molecules that recruit metal ions to function. However, nearly all previous DNAzymes generated through conventional selection methods exhibit poor metal selectivity. Here, we report an acidic *in vitro* selection strategy for isolating truly metal-specific DNAzymes. By using Ca^{2+} as the target in positive selection and a mixture of competing metal ions in counter-selection, and conducting the selections under acidic conditions to suppress metal hydrolysis, we have successfully selected an acidic RNA-cleaving DNAzyme, termed aRCD-Ca2, which is only activated by Ca^{2+} and shows no response to all other tested metal ions, including monovalent ions and chemically similar competing divalent ions (Mg^{2+}, Cu^{2+}, Zn^{2+}, Co^{2+}, Ni^{2+}, Mn^{2+} and Pb^{2+}). This represents the first acidic DNAzyme with exclusive metal selectivity. Moreover, aRCD-Ca2 exhibits fast catalytic activity, with a k_{obs} of 0.026 min^{-1} toward Ca^{2+}. A *trans*-acting aRCD-Ca2TCQ was also engineered from aRCD-Ca2 that enabled highly specific and sensitive monitoring of Ca^{2+} dynamics in HT22 cell lysosomes through a fluorescent probe. We envision that the described acidic *in vitro* selection strategy can be readily adapted to obtain more new DNAzymes with high specificity for other metal ions and advance the development of nucleic acid catalysts for a wide range of applications.

Received 7th November 2025
Accepted 14th January 2026

DOI: 10.1039/d5sc08656f

rsc.li/chemical-science

Introduction

Deoxyribozymes (or DNAzymes) are single-stranded DNA molecules with catalytic activity.[1,2] In contrast to naturally evolved protein enzymes and ribozymes, DNAzymes are isolated from large pools of random DNA sequences *via in vitro* selection, a process also referred to as systematic evolution of ligands by exponential enrichment (SELEX).[3–6] Since their first report in 1994, numerous DNAzymes that can catalyze various chemical reactions have been identified by *in vitro* selection.[7–10] One of the most extensively studied classes of DNAzymes is RNA-cleaving DNAzymes (RCDs), which catalyze RNA cleavages in a site-specific manner.[11,12]

Because metal ions are commonly recruited as cofactors for structural folding and catalysis, RCDs have been widely applied to sensing or imaging of metal ions.[13–15] However, nearly all RCDs obtained through conventional *in vitro* selection suffer from poor metal specificity, particularly difficult in distinguishing chemically similar competing ions, such as Ca^{2+} and Mg^{2+}.[16] A notable example is the 8–17 DNAzyme, which was first isolated in 1997 under simulated physiological conditions (*i.e.*, 2 mM $MgCl_2$/150 mM KCl, pH 7.5, 37 °C).[17] Although derived with Mg^{2+}, 8–17 exhibits activity with many other divalent ions, including Pb^{2+}, Zn^{2+}, Ca^{2+}, Mn^{2+}, and Co^{2+}, among others.[18,19] Recent structural studies have shown that these metals induce a similar tertiary fold of 8–17, demonstrating its non-specificity in metal binding.[20] Interestingly, the 8–17 motif has been repeatedly rediscovered under different selection conditions, including variants such as 17E (isolated with Zn^{2+}), Mg5 (isolated with histidine and Mg^{2+}) and others.[21–24] These variants share the catalytic core of 8–17 (Scheme 1a), demonstrating the difficulty in obtaining truly metal-specific DNAzymes *via* traditional *in vitro* selection. In fact, many other RCDs (*e.g.*, 10–23) suffer from poor metal specificity.[25,26]

An overlooked factor in conventional *in vitro* selection is metal hydrolysis. In aqueous environments, metal-bound water molecules deprotonate and produce metal-bound hydroxyl groups.[16] As a result, DNA is not fully exposed to free metal ions during selection under neutral conditions. Lowering pH can suppress metal hydrolysis, thus facilitating the interactions between DNA and free metal ions, potentially enhancing the isolation of specific DNAzymes for a given metal ion.

Recently, a few new DNAzymes have been selected under unconventional conditions to reveal their hidden abilities.[27–31]

[a]*School of Environmental Science and Technology, Key Laboratory of Industrial Ecology and Environmental Engineering (Ministry of Education), Dalian University of Technology, Dalian POCT Laboratory, Dalian, 116024, China. E-mail: yychang@dlut.edu.cn; zhangzijie@dlut.edu.cn; mliu@dlut.edu.cn*

[b]*Central Hospital of Dalian University of Technology, Dalian 116033, China*

[c]*School of Bioengineering, Key Laboratory of Bio-Intelligent Manufacturing (Ministry of Education), Dalian University of Technology, Dalian, 116024, China*

[d]*State Key Laboratory of Pollution Control and Resources Reuse, College of Environmental Science and Engineering, Tongji University, Shanghai, 200092, China*

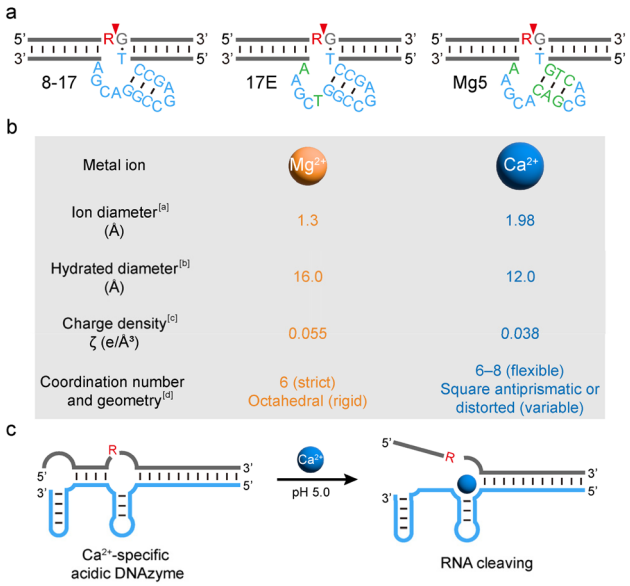

Scheme 1 Acidic *in vitro* selection of RNA-cleaving DNAzymes for discrimination between Ca^{2+} and Mg^{2+}. (a) Structures of the 8–17 DNAzyme and its variants containing the similar catalytic core motif. R denotes adenosine ribonucleotide. (b) Comparison of Mg^{2+} and Ca^{2+}. [a]Ion diameter refers to the diameter of the bare ion in the crystal. [b]Hydrated diameter refers to the effective diameter of the hydrated ion in solution. [c]Charge density is calculated as the cation's charge divided by its volume. [d]Coordination number and geometry of metal ion aqua complexes in aqueous solution. (c) Schematic presentation of the RNA-cleaving reaction catalyzed by the Ca^{2+}-specific acidic DNAzyme.

We hypothesize that, rather than conventional selections near neutral pH, selecting DNAzymes under acidic conditions could yield highly metal-specific RCDs by suppressing metal hydrolysis in a low-pH environment. In addition, acidic *in vitro* selections offer several inherent advantages. First, RNA substrates exhibit higher chemical stability under acidic conditions. For instance, the rate constant for RNA degradation at pH 6 is approximately 10-fold lower than under otherwise similar conditions at pH 7.4, which could improve the chemical stability of RNA-cleaving DNAzymes.[32] Second, acidic selection may avoid the recurrence of existing metal-nonspecific catalytic motifs such as 8–17, since DNA folding is strongly influenced by base protonation.[33,34]

To test this idea, we recruited the chemically similar Ca^{2+} and Mg^{2+} as the first case. Ca^{2+} and Mg^{2+} were chosen for three reasons: (1) they share similar properties. Both are Group 2 alkaline earth metal ions with a +2 charge and a preference for oxygen-containing ligands, making them difficult to distinguish, and many DNAzymes fail to differentiate between them;[18,24] (2) Ca^{2+} and Mg^{2+} differ in ionic radius, charge density, and coordination dynamics (Scheme 1b).[16,35–38] Ca^{2+} prefers flexible and fast-exchanging coordination (with 6–8 ligands), while Mg^{2+} exhibits rigid (mostly octahedral), slow-exchanging coordination and has a higher dehydration enthalpy due to its higher charge density;[16,36,37] (3) a Ca^{2+}-specific DNAzyme is valuable for monitoring Ca^{2+} dynamics in the acidic microenvironment of lysosomes in live cells.[39] Currently, monitoring of lysosomal components remains challenging due to the small size, acidic pH, and compartmentalization of lysosomes.

In this work, we conducted the first attempt to use acidic *in vitro* selection to isolate metal-specific DNAzymes. We have successfully isolated a Ca^{2+}-specific acidic RNA-cleaving DNAzyme, named aRCD-Ca2 (Scheme 1c), which exhibited effective catalytic activity with an observed rate constant (k_{obs}) of 0.026 min^{-1} at pH 5.0 and demonstrated excellent selectivity over other competing metal ions (Mg^{2+}, Cu^{2+}, Zn^{2+}, Co^{2+}, Ni^{2+}, Mn^{2+} and Pb^{2+}). We further developed a *trans*-acting aRCD-Ca2T-based fluorescent probe for imaging of Ca^{2+} dynamics within lysosomes in HT22 hippocampal neuron cells with high sensitivity and stability, validating its practical intracellular sensing applications.

Results and discussion

Acidic *in vitro* selection of Ca^{2+}-specific RNA-cleaving DNAzymes

Before performing the acidic *in vitro* selection, we first examined the Ca^{2+}-dependent cleavage activity of the canonical 8–17 DNAzyme and its variant 17E at pH 7.0 and 4.6. Both displayed high activity at pH 7.0 but were completely inactive at pH 4.6 (Fig. S1), thus laying the foundation for avoiding the recurrence of the 8–17 motif and generating completely new DNAzymes under acidic conditions.

The key steps in the acidic *in vitro* selection of Ca^{2+}-specific DNAzymes are illustrated in Fig. 1a. To isolate Ca^{2+}-specific DNAzymes, we performed an acidic *in vitro* selection in a low-pH selection buffer (SB) containing 50 mM glycine at pH 4.6, without using other buffer salts to avoid contamination from other metal ions. Positive selection that uses Ca^{2+} as the target metal ion and counter selection that uses a mixture of competing divalent metal ions (Mg^{2+}, Zn^{2+}, Mn^{2+}, Cu^{2+}, and Pb^{2+}) were both incorporated to promote the selection of DNAzymes with metal specificity.

The starting pool of ~10^{14} DNA molecules was initially incubated with 5 mM Ca^{2+} in the acidic selection buffer at 37 °C for positive selection. DNA molecules that cleaved the substance (FS1) in the presence of Ca^{2+} were purified using 10% denaturing polyacrylamide gel electrophoresis (dPAGE) and amplified by two rounds of PCR to regenerate the library for the next selection cycle. To enrich for highly active DNAzymes, the incubation time was gradually reduced from 12 hours to 0.5 hours, and the Ca^{2+} concentration was decreased from 5 mM to 1 mM from round 1 (R1) to round 8 (R8). Counter selection steps were introduced in rounds 6–8 to enhance the metal specificity. Additional experimental details are provided in the SI.

As illustrated in Fig. 1b, an 82-nucleotide (nt) DNA library containing a 40-nt randomized region flanked by two 21-nt primer-binding sites (PBSs) for PCR amplification was used (oligonucleotide sequences are provided in Tables S1 and S2 of the SI). The library was ligated to a 30-nt substrate FS1, which was purposely engineered with a single ribonucleotide adenosine (rA) as the intended cleavage site (R). FS1 was labeled with

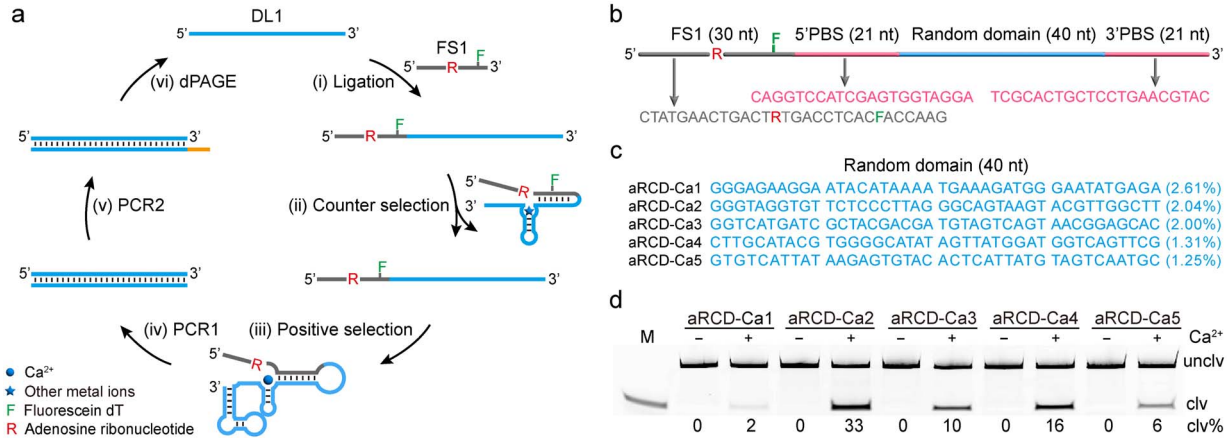

Fig. 1 Acidic *in vitro* selection of Ca^{2+}-specific RNA-cleaving DNAzymes. (a) Strategy of the acidic *in vitro* selection. (i) DNA library (DL1) was linked to a substrate (FS1). (ii) The ligation products were incubated in buffer containing 150 mM Na^+, 10 mM Mg^{2+}, 1 mM Zn^{2+}, 1 mM Mn^{2+}, 1 mM Cu^{2+}, and 0.2 mM Pb^{2+}, with 50 mM glycine at pH 4.6. Cleaved DNA molecules were discarded, and the uncleaved ones were collected. (iii) The uncleaved products were incubated in selection buffer (1× SB; 50 mM glycine, pH 4.6) with different concentrations of Ca^{2+}. Cleaved DNA molecules were subsequently collected. (iv and v) The cleaved products were amplified by PCR. (b) Library construct used for selection: a DNA library containing a 40-nt random domain and two constant primer-binding sites (PBSs) was linked to a 30-nt substrate FS1 containing an adenosine ribonucleotide (rA) as the cleavage site. FS1 was modified with fluorescein (F) for fluorescence measurement. (c) Random domain sequences of the top five selected RCD-Ca (aRCD-Ca1 to aRCD-Ca5). (d) Cleavage activity analysis of aRCD-Ca1 to aRCD-Ca5 evaluated by the cleavage yield (clv%) in 1× SB containing 0.5 mM Ca^{2+}. Reaction time: 1 h. unclv: uncleaved aRCD-Ca; clv: 5′ cleavage fragment; M: marker for the 5′ cleavage fragment. Gel band intensities were quantified using ImageQuant TL software. The uncropped gel image is provided in the SI.

fluorescein (F) at position 24 to enable fluorescent monitoring of DNAzyme cleavage during selection. Selection progress was monitored by quantifying the cleavage yield (clv%) to confirm the enrichment of Ca^{2+}-specific DNAzymes (Fig. S2). After eight rounds of selection, the cleavage products were collected and sequenced. Many candidate sequences were identified. The five top sequences in the R8 pool are shown in Fig. 1c, and they occupied 9.21% of the total population of R8. The top five candidates were designated aRCD-Ca1 through aRCD-Ca5, where "aRCD-Ca" stands for acidic RNA-cleaving DNAzyme for Ca^{2+}, and the number reflects their enrichment rank in R8. Due to sequence differences, aRCD-Ca1 to aRCD-Ca5 exhibit diverse features in their predicted secondary structures (Fig. S3).

Catalytic proficiency and metal specificity of aRCD-Ca2

We first assessed the catalytic activity of the top five candidate sequences (aRCD-Ca1 to aRCD-Ca5). Each of them was ligated to 5′-fluorescein-labeled substrate FS2 for testing. After a 1-hour incubation with 0.5 mM Ca^{2+} in acidic selection buffer, the cleaved and uncleaved products were separated *via* dPAGE, and the clv% was calculated based on the fluorescence intensity (Fig. 1d). These DNA sequences exhibited varying activities. Notably, aRCD-Ca2 showed the highest activity, achieving a clv% of 33% within 1 hour.

The predicted secondary structure of aRCD-Ca2 is shown in Fig. 2a. Since aRCD-Ca2 was selected under acidic conditions, we next examined its cleavage activity across a range of pH values (Fig. S4). The highest cleavage was achieved at pH 5.0 (clv%: 42%), close to the selection condition. Sigmoidal fitting of clv% *versus* pH revealed a transition midpoint (pH_T) of 5.33 ± 0.01 (Fig. 2b). Moreover, aRCD-Ca2 displayed a narrow response range, defined as the pH interval in which it retains 10–90% of maximal activity, spanning only ~0.4 pH units. The Hill coefficient (n_H) was determined to be 4.9 ± 0.6, indicating strong cooperative binding of protons. This high degree of cooperativity enables an ultrasensitive pH response, where small pH shifts lead to pronounced changes in the cleavage activity. This property has been effectively exploited in previous studies to track drug-induced pH changes in cellular lysosomes.[34] Notably, a gradual reduction in activity was observed between pH 5.0 and 5.6, suggesting that aRCD-Ca2 may use general acid catalysis, in which protonation is progressively suppressed as the pH increases.[40]

We next examined the cleavage kinetics of aRCD-Ca2 (Fig. S5). As shown in Fig. 2c, aRCD-Ca2 achieved a clv% of 59% within two hours of reaction in the presence of Ca^{2+} at pH 5.0 and 37 °C, with a k_{obs} of 0.026 min^{-1}. In contrast, no detectable cleavage was observed in the absence of Ca^{2+}, confirming its dependency on Ca^{2+}.

We quantitatively assessed the cleavage activity of aRCD-Ca2 across a range of Ca^{2+} concentrations (Fig. S6). As shown in Fig. 2d, aRCD-Ca2 exhibited a clear dose-dependent response to Ca^{2+} in the range of 0–300 μM, with a linear detection range between 3 and 20 μM ($R^2 = 0.991$). We next evaluated its specificity for metal ions, a key property for DNAzymes in metal detection. The cleavage activity of aRCD-Ca2 was tested in the presence of competing metal ions, including 1 mM divalent cations (Mg^{2+}, Cu^{2+}, Zn^{2+}, Co^{2+}, Ni^{2+}, and Mn^{2+}) and 150 mM monovalent cations (Na^+, K^+, and Li^+) (Fig. 2e). aRCD-Ca2 exhibits high catalytic activity exclusively in the presence of Ca^{2+}, with no detectable activity toward other metal ions. Due to the low pK_a of water coordinated to Pb^{2+}, lead ions can

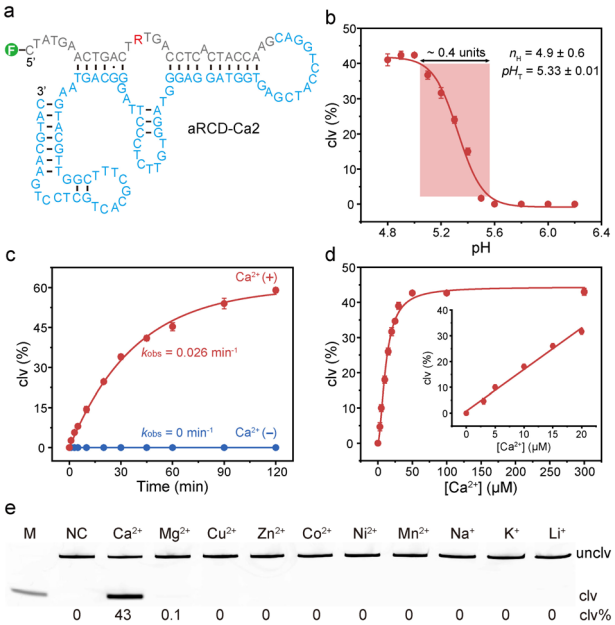

Fig. 2 Characterization of aRCD-Ca2. (a) The predicted secondary structure of aRCD-Ca2. (b) Cleavage yield (clv%) as a function of pH. Hill coefficient (n_H) and pH transition midpoint (pH_T) are indicated. (c) Cleavage kinetics of aRCD-Ca2 in the absence (blue) and presence (red) of 300 μM Ca^{2+} in 1× RB (50 mM glycine, pH 5.0). The observed rate constant (k_{obs}) is shown. (d) Cleavage activity of aRCD-Ca2 in the presence of different concentrations of Ca^{2+} in 1× RB at 37 °C for 1 h. The inset shows the linear dose–response relationship between clv% and Ca^{2+} concentration (3–20 μM; $R^2 = 0.991$). Error bars represent mean ± SD (n = three independent experiments). (e) Metal specificity of aRCD-Ca2. Reactions were conducted with 300 μM Ca^{2+} or 1 mM competing divalent metal ions (Mg^{2+}, Cu^{2+}, Zn^{2+}, Co^{2+}, Ni^{2+}, and Mn^{2+}) or 150 mM monovalent ions (Na^+, K^+, and Li^+). NC: negative control without metal ions. The uncropped gel image is provided in the SI.

efficiently hydrolyze RNA, and many DNAzymes exhibit higher activity with Pb^{2+} than with other metal ions.[16] However, under equivalent metal ion concentrations, aRCD-Ca2 shows minimal cleavage with Pb^{2+} (clv%: 3%), while retaining high selectivity for Ca^{2+} (clv%: 45%, Fig. S7). As noted, the Ca^{2+}/Pb^{2+} discrimination achieved by aRCD-Ca2 is much greater than that of the EtNa DNAzyme, which lacks the selectivity between Ca^{2+} and Pb^{2+}.[41]

The success of aRCD-Ca2 suggests that acidic *in vitro* selection can facilitate the discovery of new DNAzymes with enhanced metal specificity. In contrast, DNAzymes isolated using conventional selection under neutral conditions often struggle to distinguish similar metal ions. For example, the classical 8–17 and 10–23 DNAzymes cannot differentiate between Ca^{2+} and Mg^{2+}.[16,17] Similarly, Mg5 and 17EV1 DNAzymes also fail to discriminate between Ca^{2+} and Mg^{2+}.[22,24] In addition to ionic size and charge density, Mg^{2+} and Ca^{2+} also differ in their hydration properties and coordination flexibility. Previous theoretical calculations have shown that Mg^{2+} forms a rigid six-coordinate hydration structure with a high dehydration and water-exchange energy barrier, whereas Ca^{2+} can adopt more flexible coordination numbers (6–8) with lower water-exchange barriers.[42–47] Compared to Mg^{2+}, Ca^{2+} more readily undergoes transient coordination rearrangement, which may allow it to interact more effectively with DNA. Acidic conditions could facilitate Ca^{2+} coordination reorganization, thereby enhancing the discrimination from Mg^{2+}.

Sequence optimization of aRCD-Ca2 by nucleotide truncation

To investigate the functional importance of structural elements and improve the practicality of DNAzymes, we systematically truncated aRCD-Ca2. It was found that 32 nucleotides of aRCD-Ca2 could be removed without affecting its catalytic activity (Fig. S8). This leads to a minimized *cis*-acting version named aRCD-Ca2S (Fig. 3a). aRCD-Ca2S retains essential structural features, including a single-stranded region (SS1), four short duplexes (P1–P4), three hairpin loops (L1–L3), and four interhelical unpaired junctions (J1/2, J2/3, J3/1, and J1/4).

We next evaluated the catalytic performance of aRCD-Ca2S. It exhibited a k_{obs} of 0.022 min^{-1} and a clv% of 43% within 1 hour in 1× RB at pH 5.0 and 37 °C (Fig. S9), confirming that the truncation did not impair the catalytic efficiency of the parent aRCD-Ca2.

Based on the minimized *cis*-acting aRCD-Ca2S, we next engineered a *trans*-acting version by splitting the L1 loop of aRCD-Ca2S. The resulting construct, named aRCD-Ca2T, is

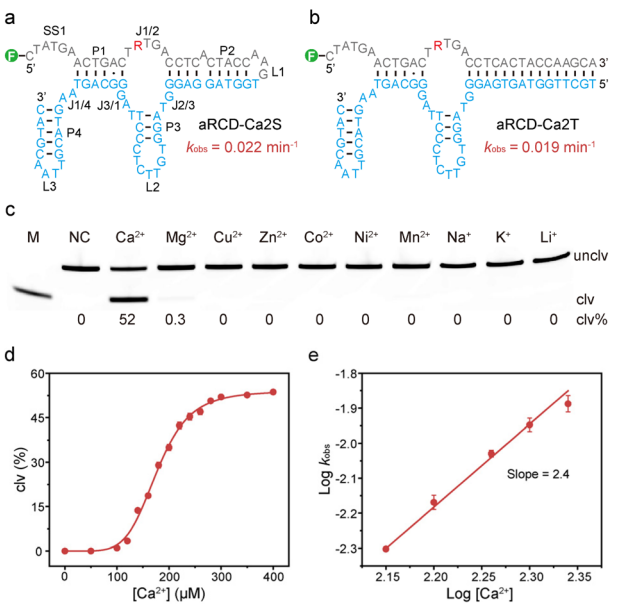

Fig. 3 Characterization of aRCD-Ca2S and aRCD-Ca2T. (a) Predicted secondary structure of minimized *cis*-acting aRCD-Ca2S. Key elements: SS (single-stranded region), P (pairing region), L (loop), and J (junction between two pairing regions). (b) Predicted secondary structure of *trans*-acting aRCD-Ca2T. (c) Selectivity of aRCD-Ca2T with 300 μM Ca^{2+} and different competing metal ions (1 mM divalent ions: Mg^{2+}, Cu^{2+}, Zn^{2+} Co^{2+}, Ni^{2+}, and Mn^{2+}; 150 mM monovalent ions: Na^+, K^+, and Li^+). The uncropped gel image is provided in the SI. (d) Cleavage activity of aRCD-Ca2T in the presence of different concentrations of Ca^{2+} in 1× RB at 37 °C. (e) Double log plots of Ca^{2+} concentration *versus* k_{obs}. Error bars represent mean ± SD (n = three independent experiments).

shown in Fig. 3b. Unlike *cis*-acting RCDs, which require ligation to their RNA substrates, *trans*-acting RCDs bind substrates through Watson–Crick base pairing. We then evaluated the catalytic activity of aRCD-Ca2T by determining its cleavage kinetics. In the presence of Ca^{2+}, aRCD-Ca2T exhibited a k_{obs} of 0.019 min^{-1}, comparable to the original aRCD-Ca2, and achieved a final cleavage yield of 53% within 1 hour (Fig. S10). This catalytic activity exceeds that of EtNa in catalyzing reactions with Ca^{2+}.[41] No cleavage activity was observed in the absence of Ca^{2+}, confirming the metal-dependent properties of aRCD-Ca2T.

We further examined the metal specificity of aRCD-Ca2T (Fig. 3c). The results showed that aRCD-Ca2T retained high selectivity for Ca^{2+} over other competing metal ions. Similarly, its cleavage activity toward Pb^{2+} remained minimal (clv%: 3%, Fig. S11). We next tested the Ca^{2+}-dependence of aRCD-Ca2T to understand its binding mechanism (Fig. 3d and S12). The clv% was measured with increasing Ca^{2+} concentrations. Curve fitting shows the sigmoidal behavior characteristic of a cooperative system, suggesting that aRCD-Ca2T requires multiple Ca^{2+} ions for efficient catalysis.

To quantitatively determine the number of Ca^{2+} ions involved in catalysis, we measured cleavage kinetics across a range of Ca^{2+} concentrations (Fig. S13a). The kinetics were fitted to determine k_{obs} at each Ca^{2+} concentration (Fig. S13b). By fitting the data to the equation $k_{obs} = k[Ca^{2+}]_n$,[48] a double-logarithmic plot of k_{obs} *versus* Ca^{2+} concentration (Fig. 3e) yielded a slope of 2.4, indicating that at least two Ca^{2+} ions are involved in the binding and catalytic process.

Characterization of the cleavage products and site selectivity of aRCD-Ca2T

Because deprotonation of the RNA 2′-hydroxyl is disfavored at low pH, the catalytic mechanism of aRCD-Ca2T under acidic conditions may differ from that at neutral pH. We therefore investigated whether RNA cleaving generates distinct terminal groups at low pH.[29] To investigate the 3′-phosphate moieties generated on the 5′-cleavage product (5′ CP), the RNA-containing substrate was incubated with aRCD-Ca2T in the presence of Ca^{2+} at pH 5.0 for 1 hour. The resulting products were then treated with various phosphodiesterases for terminal group analysis, including polynucleotide kinase (PNK), calf intestinal alkaline phosphatase (CIAP), and 2′,3′-cyclic nucleotide 3′-phosphodiesterase (CNPase). These enzymes differ in catalytic specificity: PNK possesses both 2′,3′-cyclic nucleotide 3′-phosphodiesterase and 2′/3′-phosphatase activities; CIAP exhibits only 2′/3′-phosphatase activity; while CNPase hydrolyzes 2′,3′-cyclic phosphate to 2′-phosphate.

PNK treatment reduced the gel mobility of 5′ CP, likely due to the removal of the negatively charged phosphate group (Fig. 4a, lane 4). In contrast, CIAP treatment had no effect on its migration (Fig. 4a, lane 5), and CNPase treatment similarly caused no change (Fig. 4a, lane 6). However, sequential treatment with CNPase followed by either PNK (Fig. 4a, lane 7) or CIAP (Fig. 4a, lane 8) resulted in a decreased mobility of 5′ CP.

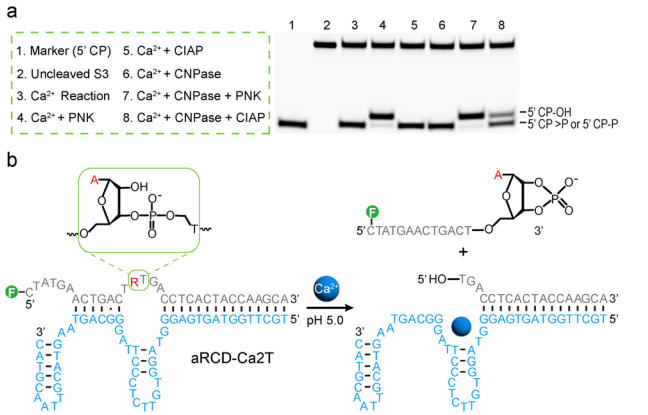

Fig. 4 Characterization of the cleavage products of aRCD-Ca2T. (a) Enzymatic digestion analysis to determine the chemical group at the 3′ end of the 5′-cleavage products (5′ CP). CP–OH represents a cleavage product with a 3′-hydroxyl group, while CP > P or CP–P indicates a 3′ terminus bearing either a 2′,3′-cyclic phosphate or a 2′-/3′-monophosphate. (b) Schematic representation of the transesterification reaction catalyzed by aRCD-Ca2T.

These results suggest that aRCD-Ca2T-mediated RNA-cleavage produces a 5′-cleavage fragment bearing a 2′,3′-cyclic phosphate and a 3′-cleavage fragment with a 5′-OH (Fig. 4b), which is similar to the cleavage products generated by conventional RCDs. To confirm the identity of the cleaved product, electrospray ionization mass spectrometry (ESI-MS) analysis of the 5′-cleavage fragment was performed, confirming that the cleavage product contains a 2′,3′-cyclic phosphate (Fig. S14).

We investigated the cleavage-site selectivity of aRCD-Ca2T. The original rAT cleavage site in the substrate was replaced with rCT, rUT, rAC, or rGC, and the catalytic activity of aRCD-Ca2T toward these substrates was examined (Fig. S15). Replacement of the adenosine ribonucleotide (rA) at the cleavage site with cytidine ribonucleotide (rC) or uridine ribonucleotide (rU) resulted in nearly undetectable cleavage activity. Similarly, substitution of the rAT cleavage site with rAC or rGC abolished catalytic activity. These results demonstrate that aRCD-Ca2T is highly specific for the rAT cleavage site. Adenosine is known to undergo protonation under acidic conditions,[40] which may contribute to the observed site selectivity of aRCD-Ca2T.

Visualizing lysosomal Ca^{2+} in HT22 hippocampal neuron cells

To convert aRCD-Ca2T into a fluorescent probe, we first employed a catalytic beacon design (named aRCD-Ca2TCQ), in which the RNA-containing substrate strand was labeled with a fluorophore (Cy5) at the 5′ end and a quencher (BHQ3) at the 3′ end of the enzyme strand. To further reduce background fluorescence, the substrate strand (CQS4) was additionally labeled with BHQ3 (Fig. 5a). In the presence of Ca^{2+}, aRCD-Ca2T can catalyze the cleavage of the substrate strand, resulting in fluorescence generation. We first evaluated the biostability of aRCD-Ca2TCQ in cell transfection medium (Opti-MEM). dPAGE results indicated that the construct remained highly stable over

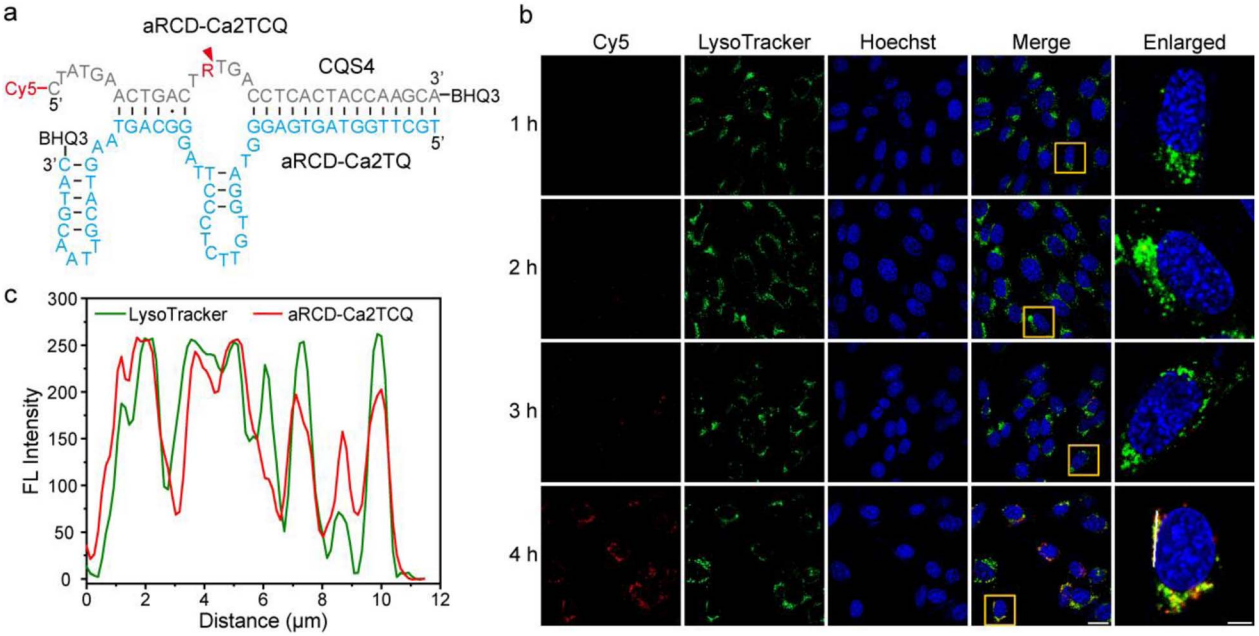

Fig. 5 Ca^{2+}-mediated activation of aRCD-Ca2TCQ in HT22 hippocampal neuron cells. (a) DNA sequences used for the construction of aRCD-Ca2TCQ. aRCD-Ca2TCQ consists of an aRCD-Ca2TQ DNAzyme strand hybridized with a substrate CQS4 strand. (b) CLSM images of HT22 hippocampal neuron cells incubated with aRCD-Ca2TCQ for 1, 2, 3, and 4 h. Hoechst 33342 used for cell nuclear fluorescence staining. Scale bars: 20 μm (merged images) and 5 μm (enlarged image). (c) Fluorescence intensity profile along the white line in the enlarged image at 4 h. HT22 hippocampal neuron cells were obtained from the Central Hospital of Dalian University of Technology.

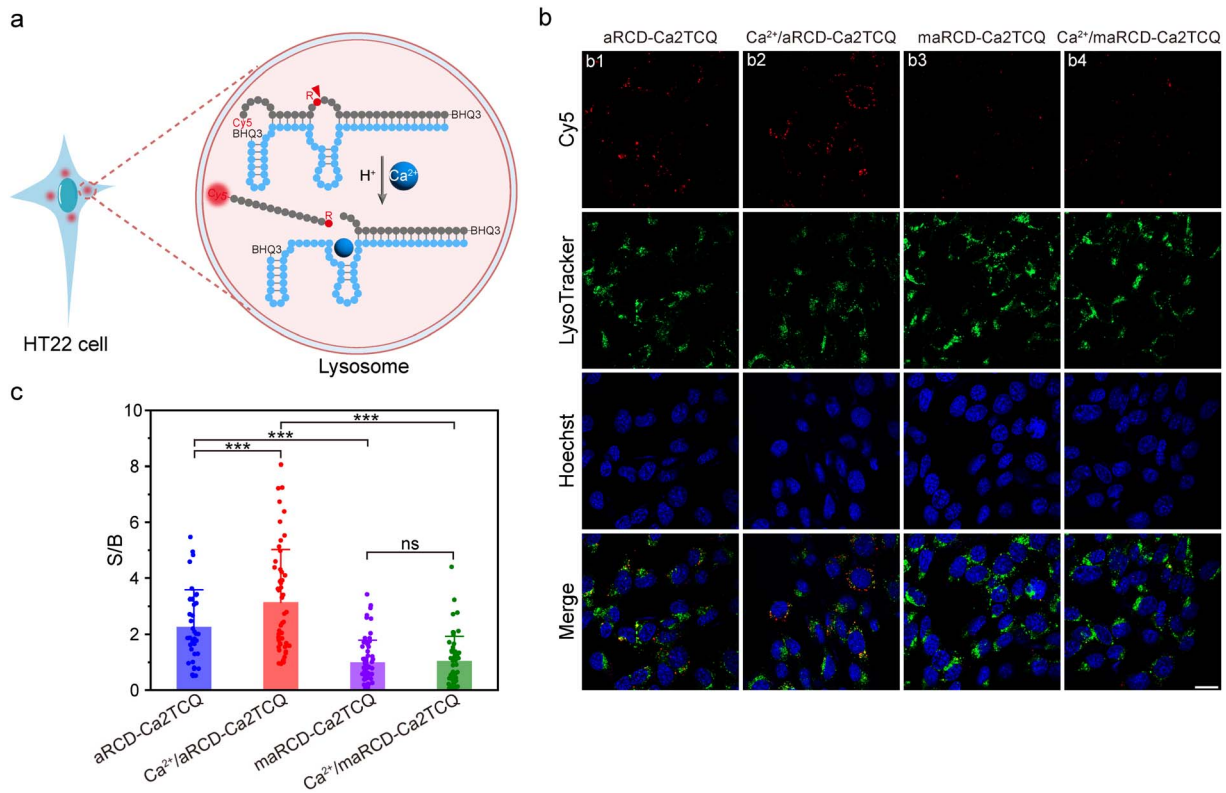

Fig. 6 aRCD-Ca2TCQ respond to lysosomal Ca^{2+} changes in HT22 hippocampal neuron cells. (a) Schematic illustration of aRCD-Ca2TCQ for imaging lysosomal Ca^{2+} in HT22 hippocampal neuron cells. (b) Representative CLSM imaging of HT22 hippocampal neuron cells under different treatment conditions: (b1) aRCD-Ca2TCQ only, (b2) pre-treated with Ca^{2+} (1 mM) and ionomycin (2 μM) for 15 min following incubation with aRCD-Ca2TCQ, (b3) maRCD-Ca2TCQ only, (b4) pre-treated with Ca^{2+} (1 mM) and ionomycin (2 μM) for 15 min following incubation with maRCD-Ca2TCQ. Hoechst 33342 was used for cell nuclear fluorescence staining. Scale bars: 20 μm. (c) Comparison of signaling magnitude (*i.e.*, S/B, defined as the fluorescence intensity in treated cells over that of maRCD-Ca2TCQ-transfected cells) in different cells in (b). Data are presented as mean ± SD (n = 36, 54, 65, and 56 cells). ***p < 0.001; ns, no significant difference. The one-way ANOVA test was used for statistical analysis.

an 8-hour incubation (Fig. S16). We also assessed its cellular compatibility in HT22 hippocampal neuron cells using a standard MTT assay, which showed no significant reduction in cell viability (Fig. S17).

Given the excellent *in vitro* performance of aRCD-Ca2T, we next investigated its potential for sensing Ca^{2+} in living cells. Lysosomes have recently been recognized as acidic Ca^{2+} reservoirs, with luminal Ca^{2+} concentrations maintained at approximately 0.5 mM—nearly 5000 times higher than that of the cytosol (~100 nM).[49] Lysosomal Ca^{2+} plays a crucial role in regulating diverse cellular processes, including vesicle fusion, intracellular signaling, transcriptional regulation, lysosomal dynamics, autophagy, and exocytosis.[50] However, the absence of Ca^{2+}-specific DNAzymes that function exclusively under acidic conditions has hindered the accurate quantification of Ca^{2+} in acidic organelles. Therefore, we investigated the potential of aRCD-Ca2T for visualizing lysosomal Ca^{2+} fluctuations in living cells.

To evaluate lysosomal colocalization, HT22 hippocampal neuron cells were incubated with aRCD-Ca2TCQ for various durations. At 4 hours post-transfection, colocalization analysis between the Cy5 and LysoTracker channels yielded a Pearson correlation coefficient of 0.80, demonstrating its strong lysosomal localization (Fig. 5b). Fluorescence intensity profiling analysis along the white line in the merged image further confirmed the spatial overlap between these two signals (Fig. 5c). We observed a gradual increase in red fluorescence in the Cy5 channel over time, indicative of DNAzyme activation. In contrast, a mutant version (maRCD-Ca2TCQ), containing critical nucleotide substitutions in the J2/3 junction (GT replaced with AA) and the J3/1 junction (TAG replaced with ATT), showed no appreciable signal increase (Fig. S18). These results demonstrate that aRCD-Ca2TCQ is specifically activated by lysosomal Ca^{2+}, enabling visualization of endogenous Ca^{2+} within lysosomes.

To verify the responsiveness of aRCD-Ca2TCQ to changes in lysosomal Ca^{2+} levels (Fig. 6a), we introduced exogenous Ca^{2+} and applied ionomycin to facilitate the equilibration of Ca^{2+} across cellular membranes.[39,51] As shown in Fig. 6b, the fluorescence observed in the Cy5 channel was attributed to the activation of aRCD-Ca2TCQ by lysosomal Ca^{2+} (Image b1). Upon Ca^{2+} treatment, a marked increase in Cy5 fluorescence intensity was observed (Image b2), confirming that the probe is capable of detecting changes in lysosomal Ca^{2+} levels. In contrast, cells transfected with the mutant maRCD-Ca2TCQ displayed minimal fluorescence signals, regardless of Ca^{2+} influx (Images b3 and b4), thus highlighting the high specificity of aRCD-Ca2TCQ for Ca^{2+}. Quantitative fluorescence analysis revealed that HT22 hippocampal neuron cells transfected with aRCD-Ca2TCQ exhibited 2.3-fold and 3.1-fold higher fluorescence intensities in the absence and presence of Ca^{2+} influx, respectively, compared to cells treated with the mutant probe (Fig. 6c). Together, these results demonstrate that aRCD-Ca2TCQ enables reliable monitoring of lysosomal Ca^{2+} fluctuations in living cells.

Conclusions

In summary, we have demonstrated an innovative approach for enhancing the metal specificity in DNAzyme evolution by harnessing acidic *in vitro* selection. While certain RCDs capable of recognizing Ca^{2+} have been reported, no Ca^{2+}-specific DNAzymes have previously been directly isolated *via in vitro* selection under acidic conditions. Leveraging this strategy, we successfully isolated a Ca^{2+}-specific aRCD from a random DNA library by performing positive selection in the presence of Ca^{2+} at low pH, followed by counter selection against competing metal ions (Mg^{2+}, Zn^{2+}, Mn^{2+}, Cu^{2+}, and Pb^{2+}). The resulting aRCD-Ca2 exhibited robust activity and exceptional discrimination against other competing metals at pH 5.0. This strategy can be readily adapted to isolate new high-specific DNAzymes for other metal ions.

Although the role of Ca^{2+} in the catalysis of aRCD-Ca2 remains to be fully elucidated, the reduced activity with increasing pH from 5.0 to 5.6 supports the notion that RNA cleavage by aRCD-Ca2 likely proceeds through general acid catalysis. The specific recognition principles and catalytic mechanisms still need to be clarified through high-resolution techniques, such as crystallography and nuclear magnetic resonance (NMR), to gain a deeper understanding of its molecular structures. We further engineered a *trans*-acting variant, aRCD-Ca2T, which displays strongly cooperative binding to Ca^{2+}, a feature that likely underlies its high metal specificity. Based on this *trans*-acting design, we developed a fluorescent probe, aRCD-Ca2TCQ, for imaging endogenous lysosomal Ca^{2+} in HT22 hippocampal neuron cells, thereby offering a highly selective potential tool for studying Ca^{2+}-mediated biological processes within lysosomes.

Together, these findings not only elucidate the potential of specific metal–DNA interactions in acidic media but also expand the toolkit for selective metal sensing in complex biological environments. Future work will focus on extending this platform to other biologically relevant metal ions and combining these DNAzymes into diagnostic and therapeutic applications.

Author contributions

P. J. was responsible for the conception and design of the study, conducted the experiments, analyzed the data, and drafted the manuscript. S. L., W. X., S. S. X., Q. Z., J. X. L., and Y. W. assisted in revising the manuscript. Y. Y. C., Z. J. Z., and M. L. contributed to the study design, provided guidance during the research, and assisted in manuscript editing. All authors read and approved the final manuscript.

Conflicts of interest

There are no conflicts to declare.

Data availability

All the data supporting this study are included in the main text and the supplementary information (SI). Supplementary information is available. See DOI: https://doi.org/10.1039/d5sc08656f.

Acknowledgements

This work was supported by the National Key R&D Program (2023YFC3711100), National Natural Science Foundation of China (NSFC; 22425602), Dalian Science and Technology Innovation Fund (2023YGZD04), Dalian Science and Technology Talent Innovation Support Program (2024RJ001) and Program of Introducing Talents of Discipline to Universities (B25041).

Notes and references

1 B. Cuenoud and J. W. Szostak, *Nature*, 1995, **375**, 611–614.
2 R. R. Breaker, *Nat. Biotechnol.*, 1997, **15**, 427–431.
3 R. R. Breaker and G. F. Joyce, *Chem. Biol.*, 1994, **1**, 223–229.
4 H. Gu, K. Furukawa, Z. Weinberg, D. F. Berenson and R. R. Breaker, *J. Am. Chem. Soc.*, 2013, **135**, 9121–9129.
5 Q. Hu, Z. Tong, A. Yalikong, L.-P. Ge, Q. Shi, X. Du, P. Wang, X.-Y. Liu, W. Zhan, X. Gao, D. Sun, T. Fu, D. Ye, C. Fan, J. Liu, Y.-S. Zhong, Y.-Z. Jiang and H. Gu, *Nat. Chem.*, 2023, **16**, 122–131.
6 T. Chang, G. Li, D. Chang, R. Amini, X. Zhu, T. Zhao, J. Gu, Z. Li and Y. Li, *Angew. Chem., Int. Ed.*, 2023, **62**, e202310941.
7 J. Shi, Q. Zhang, Y. Wu, Y. Chang and M. Liu, *Chem. Sci.*, 2024, **15**, 13452–13458.
8 X. Li, Y. Chang, Y. Wu and M. Liu, *Chem. Sci.*, 2024, **15**, 2996–3002.
9 S. K. Silverman, *Acc. Chem. Res.*, 2009, **42**, 1521–1531.
10 S. K. Silverman, *Angew. Chem., Int. Ed.*, 2010, **49**, 7180–7201.
11 B. Dou, H. Shen, Z. Li, H. Cheng and P. Wang, *Chem. Sci.*, 2025, **16**, 3470–3478.
12 D. Luo, X. Lin, Y. Zhao, J. Hu, F. Mo, G. Song, Z. Zou, F. Wang and X. Liu, *Chem. Sci.*, 2022, **13**, 5155–5163.
13 R. J. Lake, Z. Yang, J. Zhang and Y. Lu, *Acc. Chem. Res.*, 2019, **52**, 3275–3286.
14 E. M. McConnell, I. Cozma, Q. Mou, J. D. Brennan, Y. Lu and Y. Li, *Chem. Soc. Rev.*, 2021, **50**, 8954–8994.
15 C. Hong, Q. Wang, Y. Chen, Y. Gao, J. Shang, X. Weng, X. Liu and F. Wang, *Chem. Sci.*, 2021, **12**, 15339–15346.
16 W. Zhou, R. Saran and J. Liu, *Chem. Rev.*, 2017, **117**, 8272–8325.
17 S. W. Santoro and G. F. Joyce, *Proc. Natl. Acad. Sci. U. S. A.*, 1997, **94**, 4262–4266.
18 A. K. Brown, J. Li, C. M. B. Pavot and Y. Lu, *Biochemistry*, 2003, **42**, 7152–7161.
19 H. Liu, X. Yu, Y. Chen, J. Zhang, B. Wu, L. Zheng, P. Haruehanroengra, R. Wang, S. Li, J. Lin, J. Li, J. Sheng, Z. Huang, J. Ma and J. Gan, *Nat. Commun.*, 2017, **8**, 2006.
20 J. Wieruszewska, A. Pawłowicz, E. Połomska, K. Pasternak, Z. Gdaniec and W. Andrałojć, *Nat. Commun.*, 2024, **15**, 4218.
21 J. Li, W. Zheng, A. H. Kwon and Y. Lu, *Nucleic Acids Res.*, 2000, **28**, 481–488.
22 D. Faulhammer and M. Famulok, *Angew. Chem., Int. Ed.*, 1996, **35**, 2837–2841.
23 K. L. Y. Schlosser, *Biochemistry*, 2004, **43**, 9695–9707.
24 W. Zhou, Y. Zhang, J. Ding and J. Liu, *ACS Sens.*, 2016, **1**, 600–606.
25 H. Rosenbach, J. Victor, M. Etzkorn, G. Steger, D. Riesner and I. Span, *Molecules*, 2020, **25**, 3100.
26 J. Borggräfe, J. Victor, H. Rosenbach, A. Viegas, C. G. W. Gertzen, C. Wuebben, H. Kovacs, M. Gopalswamy, D. Riesner, G. Steger, O. Schiemann, H. Gohlke, I. Span and M. Etzkorn, *Nature*, 2022, **601**, 144–149.
27 Z. Liu, S. H. Mei, J. D. Brennan and Y. Li, *J. Am. Chem. Soc.*, 2003, **125**, 7539–7545.
28 S. A. Kandadai, *Nucleic Acids Res.*, 2005, **33**, 7164–7175.
29 S. A. Kandadai, W. W. K. Mok, M. M. Ali and Y. Li, *Biochemistry*, 2009, **48**, 7383–7391.
30 Y. Shen, J. D. Brennan and Y. Li, *Biochemistry*, 2005, **44**, 12066–12076.
31 Q. Zhou, G. Zhang, Y. Wu, Q. Zhang, Y. Liu, Y. Chang and M. Liu, *J. Am. Chem. Soc.*, 2023, **145**, 21370–21377.
32 Y. Li and R. R. Breaker, *J. Am. Chem. Soc.*, 1999, **121**, 5364–5372.
33 Y. Lee, R. Roy, S. Gu, S. B. Shetty, A. K. Rangadurai and H. M. Al-Hashimi, *J. Am. Chem. Soc.*, 2025, **147**, 19643–19666.
34 P. Jia, Q. Meng, Q. Zhang, R. Zhang, Z. Zhang, J. Li, X. Wang, Y. Liu, Y. Chang and M. Liu, *Anal. Chem.*, 2025, **97**, 9378–9385.
35 E. Koculi, C. Hyeon, D. Thirumalai and S. A. Woodson, *J. Am. Chem. Soc.*, 2007, **129**, 2676–2682.
36 T. Ikeda, M. Boero and K. Terakura, *J. Chem. Phys.*, 2007, **127**, 074503.
37 I. Persson, *Liquids*, 2022, **2**, 210–242.
38 Z. Sun, W. Zhang, M. Ji, R. Hartsock and K. J. Gaffney, *J. Phys. Chem. B*, 2013, **117**, 12268–12275.
39 N. Narayanaswamy, K. Chakraborty, A. Saminathan, E. Zeichner, K. Leung, J. Devany and Y. Krishnan, *Nat. Methods*, 2018, **16**, 95–102.
40 L. Ma, S. Kartik, B. Liu and J. Liu, *Nucleic Acids Res.*, 2019, **47**, 8154–8162.
41 W. Zhou, R. Saran, P.-J. J. Huang, J. Ding and J. Liu, *ChemBioChem*, 2017, **18**, 518–522.
42 Y. I. Neela, A. S. Mahadevi and G. N. Sastry, *Struct. Chem.*, 2013, **24**, 637–650.
43 D. Rutkowska-Zbik, M. Witko and L. Fiedor, *J. Mol. Model.*, 2013, **19**, 4661–4667.
44 J. Weston, *The Chemistry of Organomagnesium Compounds*, 2008, pp. 315–367.
45 S. F. Lincoln, D. T. Richens and A. G. Sykes, *Compr. Coord. Chem. II*, 2003, **1**, 515–555.
46 M. Pavlov, P. E. M. Siegbahn and M. Sandström, *J. Phys. Chem. A*, 1998, **102**, 219–228.
47 P.-C. Cheng, F.-S. Tseng, C.-T. Yeh, T.-G. Chang, C.-C. Kao, C.-H. Lin, W.-R. Liu, J.-S. Chen and V. Zima, *CrystEngComm*, 2012, **14**, 6812–6822.

48 P.-J. J. Huang, D. de Rochambeau, H. F. Sleiman and J. Liu, *Angew. Chem., Int. Ed.*, 2020, **59**, 3573–3577.
49 J. Yang, Z. Zhao, M. Gu, X. Feng and H. Xu, *Protein Cell*, 2018, **10**, 8–19.
50 C. Settembre and R. M. Perera, *Nat. Rev. Mol. Cell Biol.*, 2023, **25**, 223–245.
51 Y. Kuronuma, Y. Shindo, R. Kumada, A. Sakama, D. Citterio, K. Oka and Y. Hiruta, *ACS Chem. Neurosci.*, 2025, **16**, 649–658.